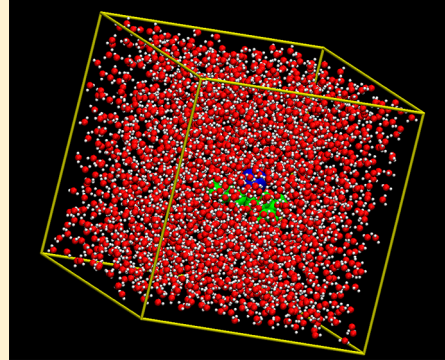


# Pairing Mechanism among Ionic Liquid Ions in Aqueous Solutions: A Molecular Dynamics Study

Harsha V. R. Annareddy and Liem X. Dang\*

Physical Sciences Division, Pacific Northwest National Laboratory Richland, Washington 99352, United States

**ABSTRACT:** In this study, we carried out molecular dynamics simulations to examine the molecular mechanism for ionic liquid pair association in aqueous solutions. We chose the commonly studied imidazolium-based ionic liquid pairs. We computed potentials of mean force (PMF) for four systems: 1,3-dimethylimidazoliumchloride, 1,3-dimethylimidazolium iodide, 1-methyl-3-octylimidazolium chloride, and 1-methyl-3-octylimidazolium iodide. Our PMF studies show a stronger interaction for the ion pairs of systems involving dimethylimidazolium as the cation species compared with that of the systems containing octylimidazolium. This result indicates a decrease in ion-pair association as the cation alkyl tail length increases. We also studied the kinetics of ion-pair dissociation using different rate theories such as the Grote–Hynes and Kramer's theories. As expected, the computed rate results significantly deviated from results obtained from transition state theory because it does not account for dynamical solvent effects. Dissociative barrier curvatures are found to be very small for the systems investigated because the transmission coefficients computed using Grote–Hynes theory and Kramer's theory are approximately equal. Our analysis of the rotational dynamics of cations revealed that the time scales for molecular reorientation are longer for cations with longer alkyl tails.



## I. INTRODUCTION

Room-temperature ionic liquids (RTILs) are molten salts under ambient conditions. In general, RTILs are defined as salts with melting points below 100 °C. Research on RTILs is expanding rapidly. With many desirable properties, such as low volatility, high thermal stability, good electrical and thermal conductivity, wide electrochemical windows, and ability to solubilize a variety of materials, RTILs are becoming important components in advanced processes and devices with various applications. Because a large number of RTILs with varying physical properties can be made by combining various cations and anions, they often are referred to as tailor-made designer materials. However, the high viscosity of RTILs is a problem in some processes. Results from recent studies indicate that a mixture of ionic liquids and conventional solvents could solve this problem.<sup>1–4</sup> Water is the most common cosolvent used for RTILs. Ironically, for a long time, water was considered to be an impurity for RTILs; however, recent studies have shown the potential of RTIL and water mixtures as solvents for biopolymers.<sup>1,5,6</sup>

Several studies have been performed to explore the nature of RTIL+water mixtures.<sup>7–16</sup> Adding small amounts of water to RTILs dramatically alters physical properties such as conductivity and viscosity.<sup>17,18</sup> The structural organization and nanoscale ordering in RTILs are active research areas. Both experimental and simulation studies showed that the presence of water as a cosolvent significantly alters the local structure in RTILs.<sup>10,19–21</sup>

With the growing interest in RTIL and cosolvent mixtures, our intent in this study was to provide a molecular-level

understanding of ion association between RTIL ions in water. To accomplish this, we used a potential of mean force (PMF) approach to study the molecular mechanism of ion-association processes. We studied four different imidazolium-based RTILs. Combinations of ions were chosen to study the effects of anion and cation chain length on the pairing processes. We also conducted kinetic studies of ion-pair association using various rate theories. We concluded that the computed rate results significantly deviated from results obtained from transition state theory (TST) because it does not account for dynamical solvent effects. In addition, our analysis of rotational dynamics of cations shows that the time scales for molecular reorientation are longer for cations with longer alkyl tails. We should note here that Pratt and coworkers reported a similar study of the formation of 1-hexyl-3-methylimidazolium and tetrafluoroborate ions in *n*-pentanol.<sup>21</sup> They probably used *n*-pentanol as a solvent because of its relation to engineering applications of ionic liquids. Some of their conclusions are similar to conclusions we reached in our study.

## II. METHODS AND SIMULATIONS

Molecular dynamics (MD) simulations of four RTIL ion pairs [dmim][Cl], [dmim][I], [omim][Cl], and [omim][I] in water were performed using polarizable potential models. A modified version of the Amber9 package was used to perform our MD

Received: May 16, 2013

Revised: June 19, 2013

Published: June 25, 2013



simulations.<sup>22</sup> Polarizable force-field parameters for the RTIL ions and water were those developed previously in our group.<sup>23–25</sup> The [dmim]Cl system contains 2000 water molecules, and the [dmim][I] system contains 1900 water molecules. The [omim][Cl] system contains 2600 water molecules, and the [omim][I] system contains 2500 water molecules. All of the systems are pre-equilibrated for several nanoseconds in an NPT ensemble at a temperature of 300 K and 1 atm pressure before the production runs.

To understand the ion-pair association between RTIL ions in water, we used a constrained MD technique.<sup>26,27</sup> Using this approach, we evaluated the free-energy profiles as a function of the center-of-mass separation between the ions. Equation 1 is used to compute the ion–ion mean force for various solvent configurations.

$$F(r) = \frac{1}{2} \langle \vec{r}_s \cdot (\vec{F}_A - \vec{F}_B) \rangle \quad (1)$$

Here,  $\vec{F}_A$  and  $\vec{F}_B$  are the forces acting on ions A and B respectively. The term  $\vec{r}_s$  is the unit vector along AB and can be expressed as

$$\vec{r}_s = \frac{\vec{r}_{AB}}{|\vec{r}_A - \vec{r}_B|} \quad (2)$$

The PMF,  $W(r)$ , is calculated using the mean force obtained from eq 1.

$$W(r) = - \int_{r_0}^r \langle F(r) \rangle dr \quad (3)$$

In this study, we computed PMFs along the center-of-mass separation between the two ions. We carried out a series of MD simulations at different ion-separation distances with increments of 0.25 Å. All of these simulation runs were performed in a NVT ensemble at temperature of 300 K, with periodic boundary conditions applied in all three directions with a time step of 2 fs. We used the particle mesh Ewald summation technique to handle the long-range electrostatic interactions<sup>28</sup> and the SHAKE algorithm to fix the internal geometry of the solvent.<sup>29</sup> For every ion-separation distance, we performed MD simulations over a 10-ns duration, and  $F(r)$  was averaged over the last 8 ns.

### III. RESULTS AND DISCUSSION

We begin with a discussion of gas-phase interactions between the ions and between the ions and water at room temperature. In Figure 1a, we present the interaction energies between the ion pairs in the gas phase as a function of the center-of-mass separation. The interaction energy at each separation is an average over various conformations. This plot clearly shows that the interaction potential for the [dmim][Cl] ion pair has a deeper minimum and, hence, a stronger interaction energy in the gas phase compared with that of the [dmim][I] pair. The position of the minimum for [dmim][Cl] is at 3.4 Å, and as would be expected, the minimum is at smaller separation distance than that of [dmim][I] (3.9 Å). This shift in the potential minima results from the larger radius of the iodide ion compared with the chloride ion. In Figure 1b, we show interaction energy plots as a function of center-of-mass separation between the ions and water. As expected, the chloride ion has deeper minima compared with the iodide ion. Similar to Figure 1a, a right shift in potential minima for the iodide–water case is seen. The potential minimum of the

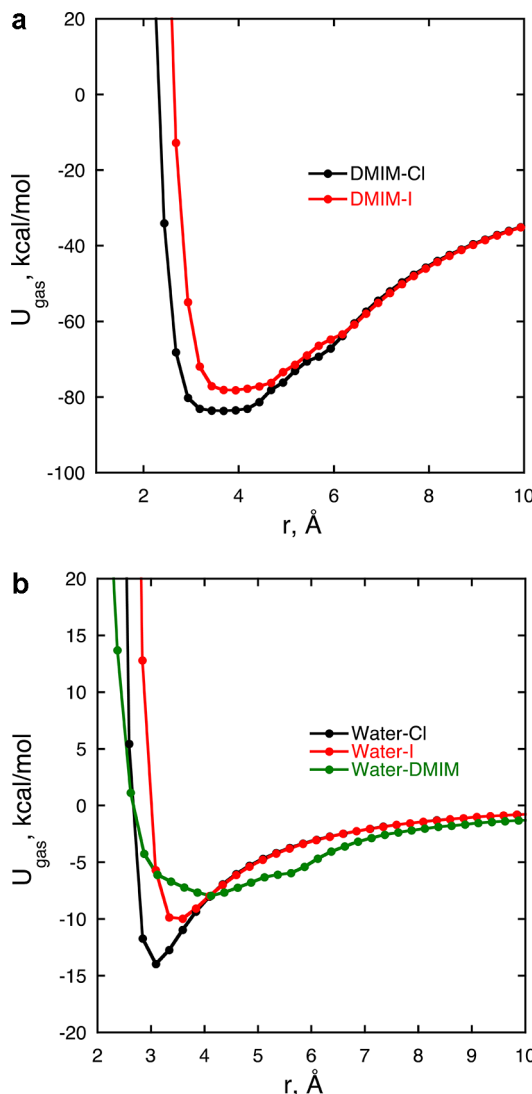


**Figure 1.** Gas-phase interaction energy as a function of center-of-mass separation. (a) [dmim][Cl], [dmim][I]. (b) [dmim]–water, iodide–water, and chloride–water.

dmim–water pair is less deep compared with iodide and chloride. In addition, it can be seen that because of the larger size and nonspherical shape of the ion the potential well for the dmim is significantly wide in comparison with the iodide and chloride cases.

In Figure 2, we present the PMF plots as a function of center-of-mass separation. It is clear to us that the PMFs for the ion pairs containing [dmim] as the cation have deeper minima compared with the corresponding [omim]-based RTILs. This demonstrates that the cations with shorter alkyl tails are more strongly associated with the anions in water. Both of the [omim] RTILs have very shallow minima and do not show any noticeable ion-pair association. In general, because of the competition between water and the ionic liquid pairs, the PMFs of [dmim][I] and [omim][I] have slightly deeper minima compared with the corresponding [dmim][Cl] and [omim][Cl].

When comparing the PMF plots of [dmim][Cl] and [dmim][I] ion pairs, we notice that the PMF minimum for the [dmim][I] is slightly deeper compared with [dmim][Cl]. This observation is contrary to the trend noticed in the gas-

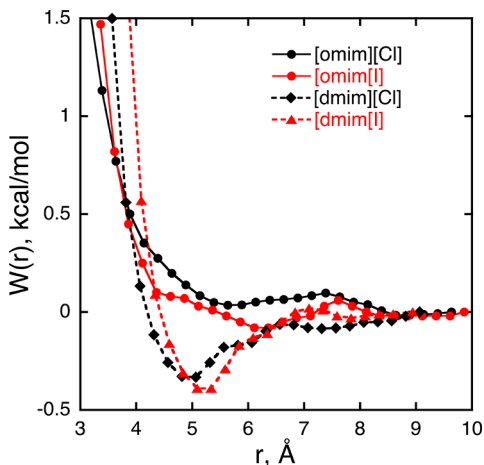


**Figure 2.** Computed PMFs for [dmim][Cl], [dmim][Cl], [omim][Cl], and [omim][I] in aqueous solutions.

phase interaction potential plots where we observe a significantly deeper minimum for [dmim][Cl]. Another interesting feature noted upon careful comparison of Figure 1a (gas-phase plots for [dmim][Cl] and [dmim][I]) and Figure 2 (PMF in water for [dmim][Cl] and [dmim][I]) is the PMF minimum in water, which is shifted toward longer separation distances compared with the minima in gas-phase plots. The higher affinity of iodide for both of the cations in water agrees with Collins empirical law of matching water affinities.<sup>30–32</sup> According to Collin's law, the relative affinity of ions in aqueous solution depends on the matching of cation and anion sizes and their charge densities. Also, the enthalpy of hydration for [dmim]<sup>+</sup> is closer to iodide than chloride. So on a water affinity scale, [dmim]<sup>+</sup> is closer to iodide compared with chloride. A similar kind of discussion is reported for the aqueous solutions of alkyl halides.<sup>33,34</sup> The depths of the PMF minima are comparable to the previous studies by Raju and Balasubramanian on dilute aqueous solutions of the [bmim][PF<sub>6</sub>] system.<sup>12</sup> The mechanism of ion-pair association and its strength in solutions is a complex phenomenon that depends on a delicate interplay of several factors, such as electrostatics and the size and structure of ions. Similar to the gas-phase plots, the shift in the minima of [dmim][I] results from the larger size of the iodide ion compared with the chloride ion. Figure 3 illustrates the ionic-liquid/water systems used to compute the PMFs.

We also computed the spatial distribution plots using the trajectories in which the center of mass separation is constrained to a particular distance. These plots provide insight into how the water structures round the ion pair along the reaction coordinate. In Figure 4, we show the spatial distribution of water and anion around the cations at the PMF minimum. The ring portion of the cations is more polar than the alkyl tails; therefore, because of strong electrostatic interactions, all of these plots clearly show a favorable binding of water as well as anions to the ring portion of the cations. The PMF plots of [dmim]<sup>+</sup> systems show local minima around ~6 Å. For [dmim][Cl], the local minimum is at 6.06 Å, and for [dmim][I], it is at 6.34 Å. The ion-pair coordination at this separation distance is depicted using the spatial distribution plots in Figure 5. The anion coordination with the cation at this local minimum is quite different compared with the global minima.

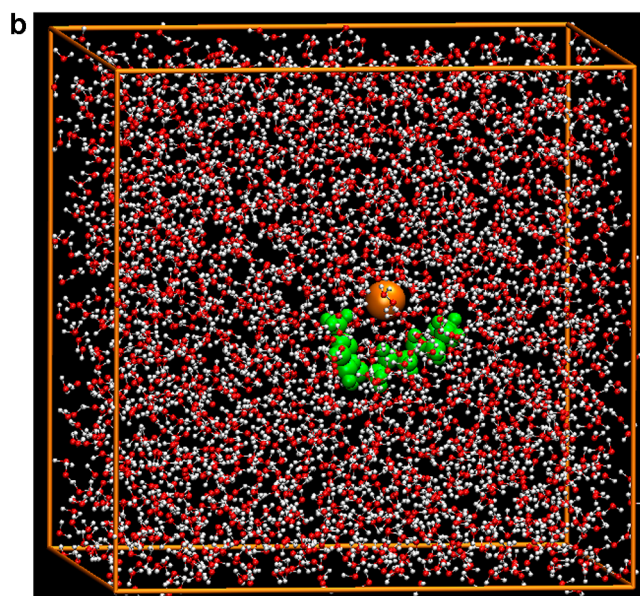
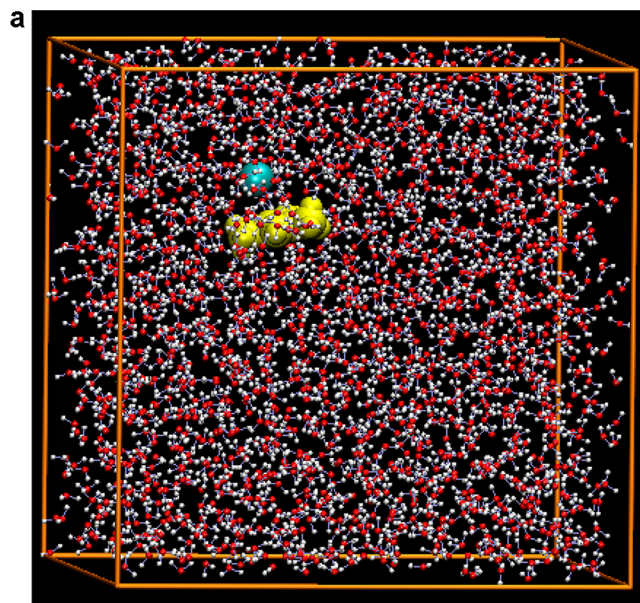


**Figure 3.** Ionic-liquid/water systems used to compute PMFs.

To understand the kinetics of ion-pair association, we applied various rate theories to our systems. According to the TST, the rate constant can be computed using the computed PMFs and eq 4<sup>27,35,36</sup>

$$k^{\text{TST}} = \sqrt{\frac{k_B T}{2\pi\mu}} \frac{(r^*)^2 e^{-\beta W(r^*)}}{\int_0^{r^*} r^2 e^{-\beta W(r)} dr} \quad (4)$$

where  $r^*$  is defined as the position of the barrier top,  $\mu$  is the ion-pair reduced mass,  $k_B$  is the Boltzmann constant, and  $T$  is the temperature. It is well known that the TST significantly overestimates the dissociation rates because of the assumption that once the reactive species reach the transition state they will directly end up on the product side without recrossing back to the reactants. Well-known corrections to the TST are Kramer's theory<sup>37</sup> and the GH theory.<sup>35,38</sup> Both of these theories provide the transmission coefficient,  $\kappa$ , to correct the TST. The

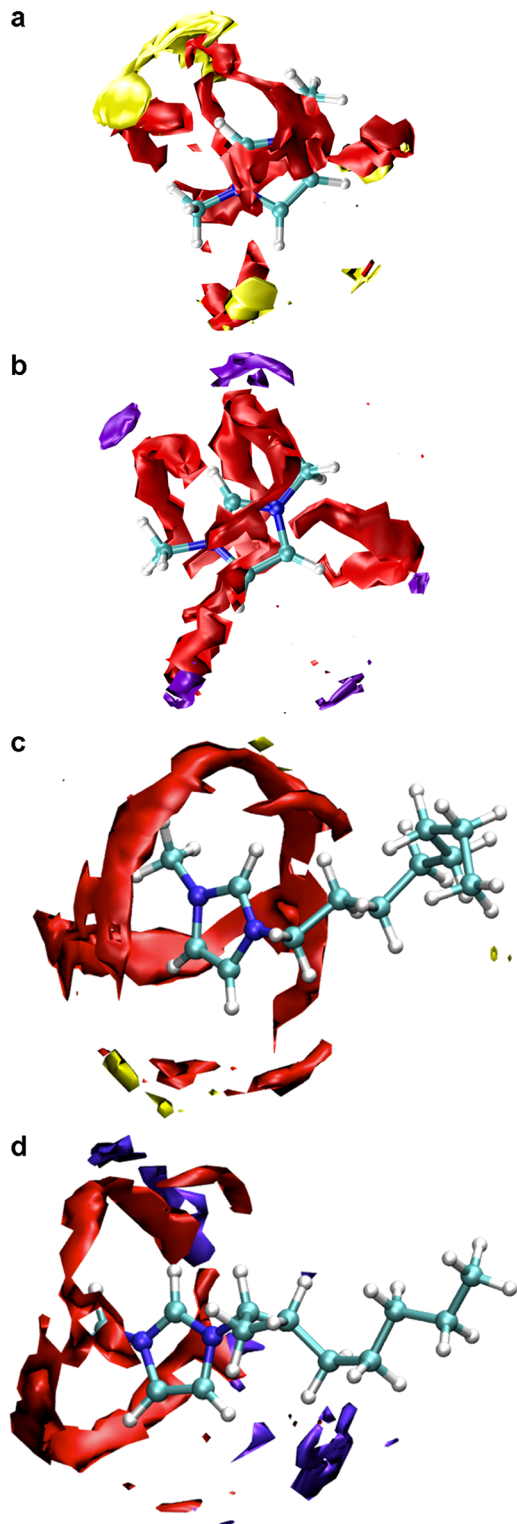


**Figure 4.** Spatial distributions of water and anion at the minima of PMF of (a) [dmim][Cl]. Chloride density is shown in yellow and oxygen atoms of water are shown in red. (b) [dmim][I] iodide density is shown in violet and oxygen atoms of water are shown in red. (c) [omim][Cl] chloride density shown in yellow and oxygen atoms of water are shown in red (d) [omim][I] iodide density is shown in violet and oxygen atoms of water are shown in red.

corrected rate constant  $k$  is given by  $k = k k^{\text{TST}}$ . According to the GH theory, the transmission coefficient is computed using eq 5

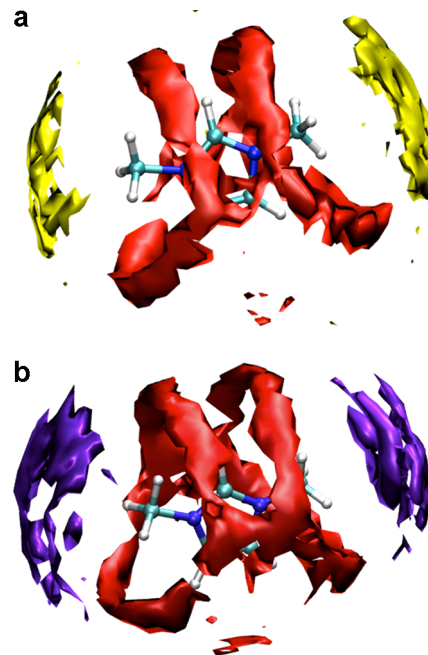


**Figure 5.** Spatial distributions at the local minima (a) [dmim][Cl] at 6.06 Å separation distance between the ions and (b) [dmim][I] at 6.34 Å separation distance between the ions.

$$\kappa_{\text{GH}} = \left( \kappa_{\text{GH}} + \int_0^\infty dt \frac{\zeta(t)}{\omega_b} e^{-\omega_b \kappa_{\text{GH}} t} \right)^{-1} \quad (5)$$

where  $\omega_b$  is the barrier frequency and  $\zeta(t)$  is the friction kernel defined by the time correlation function of the fluctuating force ( $F(t, r)$ ) on the reaction coordinate due to the solvent. The term  $\zeta(t)$  is computed by constraining the reaction coordinate at  $r^*$ .

$$\zeta(t) = \frac{1}{\mu k_b T} \langle R(t, r^*) \cdot R(0, r^*) \rangle \quad (6)$$

$$R(t, r) = F(t, r) - \langle F(t, r) \rangle \quad (7)$$

The GH theory transmission coefficient involves the frequency component of the time-dependent friction,  $\zeta(t)$ , at the Laplace frequency,  $\omega_b \kappa_{\text{GH}}$ , relevant in the barrier region. Neglecting the frequency dependence in eq 5 gives the Kramer's transmission coefficient, as shown in eq 8.

$$\kappa_{\text{Kr}} = \sqrt{1 + \left( \frac{\zeta}{2\omega_b} \right)^2} - \frac{\zeta}{2\omega_b} \quad (8)$$

Here  $\zeta$  is a constant friction coefficient that can be computed as  $\int_0^\infty \zeta(t) dt$ .

In Figure 6, we show plots of un-normalized, time-dependence friction kernels of ionic liquid pairs in water. In all cases, there are two distinct decay time scales. Both time scales show an initial rapid decay lasting for  $\sim 0.1$  ps, followed by a longer time decay that lasts for a few picoseconds. We can conclude from the data in both figures that the mass of iodide made the computed time dependence friction decay slightly slower when compared with that of chloride.

The rate constants computed from various theories are listed in Table 1. First, we compare the TST rate constants for [dmim][Cl] and [dmim][I]. The rate constant for [dmim][Cl] is greater than that for [dmim][I], indicating a faster rate of

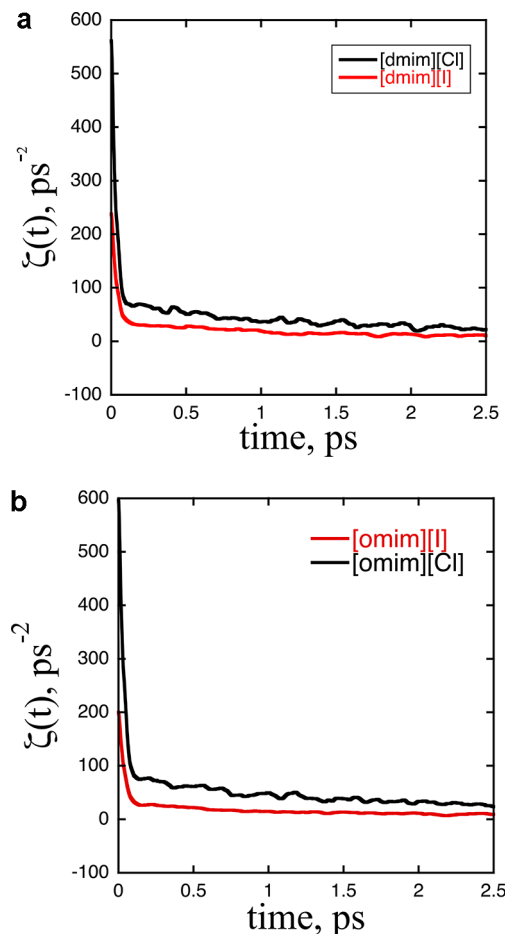


**Figure 6.** (a) Computed friction kernels for  $[\text{dmim}][\text{Cl}]$  and  $[\text{dmim}][\text{I}]$ . (b) Computed time dependence friction kernels for  $[\text{omim}][\text{Cl}]$  and  $[\text{omim}][\text{I}]$  in water.

**Table 1. Results from Rate Theories**

	$[\text{dmim}]$ [Cl]	$[\text{dmim}]$ [I]	$[\text{omim}]$ [Cl]	$[\text{omim}]$ [I]
barrier position, $r_a$ ( $\text{\AA}$ )	6.56	7.09	7.38	7.61
TST rate constant, $k^{\text{TST}}$ ( $\text{ps}^{-1}$ ), for ion-pair dissociation	0.57	0.32	0.53	0.30
barrier frequency, $\omega_b$ ( $\text{ps}^{-1}$ )	6.8	5.6	1.8	1.5
Kramer's theory transmission coefficient, $\kappa_{\text{Kr}}$	0.06	0.04	0.01	0.03
GH's theory transmission coefficient, $\kappa_{\text{GH}}$	0.07	0.03	0.01	0.02

reaction for  $[\text{dmim}][\text{Cl}]$ . This can be explained based on the barrier heights. According to TST theory, the higher the activation barrier, the slower the reaction rate. The PMF plots clearly indicate a higher barrier height for  $[\text{dmim}][\text{I}]$  when compared with that of  $[\text{dmim}][\text{Cl}]$ . Therefore, the rate of ion pair dissociation reaction for  $[\text{dmim}][\text{I}]$  is slower compared with  $[\text{dmim}][\text{Cl}]$ . The same argument could be used to explain the trend noticed in rate constants of  $[\text{omim}]$  systems.

The corrected rate constant  $k$  is given by  $k = \kappa k^{\text{TST}}$ , where  $\kappa$  is the transmission coefficient that adjusts the rate constant  $k^{\text{TST}}$  from TST. We computed transmission coefficients using both Kramer's theory and the GH theory and the results also are included in Table 1. We observe that the barrier frequency,  $\omega_b$ , decreases (from 6.8 to 1.5) from  $[\text{dmim}]$  to  $[\text{omim}]$ . Also, these values are found to be very low when compared with the

ion pair dissociative barrier frequencies for alkyl halides and other salts that were previously studied.<sup>27,36,39–41</sup> Because of small barrier curvatures, the reaction system is exposed to friction for a longer time and solvent effectively induces the recrossings, thus significantly reducing the rate of reaction compared with the TST. The small transmission coefficient values for both the GH theory and Kramer's theory reported in Table 1 corroborates this argument. Also, as can be seen from Table 1, the transmission coefficient values computed from the GH theory are very close to Kramer's theory values ( $\kappa_{\text{GH}} \approx \kappa_{\text{Kr}}$ ). This trend also is due to the small barrier curvatures; when  $\omega_b \rightarrow 0$ , then  $\kappa_{\text{GH}} \rightarrow \kappa_{\text{Kr}}$ . This is one of the cases of GH theory where the decay of the friction kernel  $\zeta(t)$  is faster compared with the time scale of the reaction coordinate motion over the barrier.<sup>27,36,42</sup>

However, we would like to mention that the rate-constant trends we observed also depend on the chosen reaction coordinate. Because of very long alkyl tails and large asymmetric structure of the cation, the center-of-mass separation may not be an ideal reaction coordinate for the  $[\text{omim}]$  system. To be consistent, we chose the same reaction coordinate for both systems. In future studies, we plan to investigate appropriate reaction coordinates.

We also studied the translational and rotational dynamics of the cations in water. In Figure 7a, we show the rotational correlation functions along three-body fixed axes for both  $[\text{dmim}]$  and  $[\text{omim}]$  cations. The axis labeled 1 is the vector joining the two nitrogen atoms in the cation ring. The axis labeled 2 is the vector perpendicular to axis 1; it passes through the carbon atom between two nitrogen atoms and is also in the

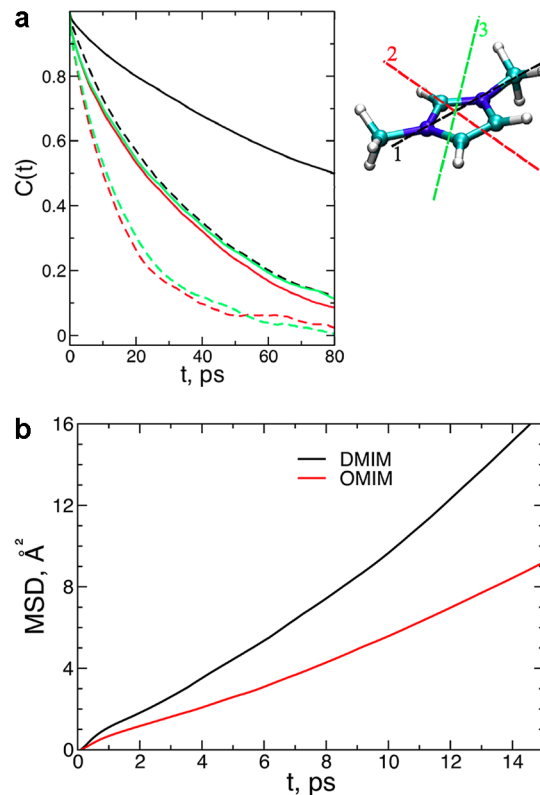


**Figure 7.** (a) Rotational correlation function along the three different body fixed axis for the two cations. Dashed lines are for  $[\text{dmim}]$  and the solid lines are for  $[\text{omim}]$ . The plots are color-coded to match the body fixed axis as shown. (b) Mean-squared displacement.

plane of imidazolium ring. The axis labeled 3 is perpendicular to vectors 1 and 2 and hence also perpendicular to the ring. A graphical representation of all three-body fixed axes is also depicted in Figure 7a. The autocorrelation functions of all three axes decay faster for [dmim] than for [omim]. The reason for this is hindered rotational motion due to the presence of longer alkyl tails. Also, as expected in both cases, decay of the correlation function along axis 1 is slower than that along axes 2 and 3 because it requires reorientation along the longest molecular axis. In Figure 7b, we show the mean-squared displacement, which clearly shows that the [dmim] cation is more diffusive than the [omim] cation.

## IV. CONCLUSIONS

We present the results of our study of the molecular mechanism of ion-pair association of various RTIL ions in water. We studied anion dependence and cation tail-length dependence. Our results indicate that ion association decreases with alkyl tail length. For both of the cation combinations, iodide shows slightly favorable association compared with chloride. Our PMF studies show a stronger interaction for the ion pairs of the systems involving [dmim] as the cation compared with that of the systems containing [omim]. This result illustrates that the ion-pair association decreases as the cation alkyl tail length increases. We also studied the kinetics of ion-pair dissociation using different rate theories such as the GH theory and Kramer's theory. Our general conclusion is that the computed rate results significantly deviate from the TST results because of very small barrier curvatures. Our analysis of rotational dynamics of cations shows that the time scales for molecular reorientation are longer for cations with longer alkyl tails.

## AUTHOR INFORMATION

### Notes

The authors declare no competing financial interest.

## ACKNOWLEDGMENTS

This work was supported by the U.S. Department of Energy (DOE), Office of Basic Energy Sciences (BES), Division of Chemical Sciences, Geosciences, and Biosciences. Pacific Northwest National Laboratory is a multiprogram national laboratory operated for DOE by Battelle. The calculations were carried out using computer resources provided by BES.

## REFERENCES

- (1) Yang, Q.; Xing, H.; Su, B.; Yu, K.; Bao, Z.; Yang, Y.; Ren, Q. *Chem. Eng. J.* **2012**, *181*, 334.
- (2) Jacquemin, J.; Husson, P.; Padua, A. A. H.; Majer, V. *Green Chem.* **2006**, *8*, 172.
- (3) Chaban, V.; Voroshlyova, I.; Kalugin, O.; Prezhdo, O. *J. Phys. Chem. B* **2012**, *116*, 7719.
- (4) Dupont, J.; de Souza, R.; Suarez, P. *Chem. Rev.* **2002**, *102*, 3667.
- (5) Khupse, N.; Kumar, A. *J. Phys. Chem. A* **2011**, *115*, 10211.
- (6) Chaban, V. V.; Prezhdo, O. V. *J. Phys. Chem. Lett.* **2011**, *2*, 2499.
- (7) Klähn, M.; Stüber, C.; Seduraman, A.; Wu, P. *J. Phys. Chem. B* **2010**, *114*, 2856.
- (8) Ries, L.; Do Amaral, F.; Matos, K.; Martini, E.; de Souza, M.; de Souza, R. *Polyhedron* **2008**, *27*, 3287.
- (9) Annapureddy, H. V. R.; Hu, Z.; Xia, J.; Margulis, C. J. *J. Phys. Chem. B* **2008**, *112*, 1770.
- (10) Sturlaugson, A.; Fruchey, K.; Fayer, M. *J. Phys. Chem. B* **2012**, *116*, 1777.
- (11) Bhargava, B. L.; Yasaka, Y.; Klein, M. L. *Chem. Commun.* **2011**, *47*, 6228.
- (12) Raju, S. G.; Balasubramanian, S. *J. Phys. Chem. B* **2009**, *113*, 4799.
- (13) Danten, Y.; Cabaco, M. I.; Besnard, M. *J. Phys. Chem. A* **2009**, *113*, 2873.
- (14) Zhong, X. J.; Fan, Z.; Liu, Z. P.; Cao, D. P. *J. Phys. Chem. B* **2012**, *116*, 3249.
- (15) Umebayashi, Y.; Jiang, J. C.; Shan, Y. L.; Lin, K. H.; Fujii, K.; Seki, S.; Ishiguro, S. I.; Lin, S. H.; Chang, H. C. *J. Chem. Phys.* **2009**, *130*, 124503.
- (16) Danten, Y.; Cabaco, M. I.; Besnard, M. *J. Mol. Liq.* **2010**, *153*, 57.
- (17) Khupse, N.; Kumar, A. *J. Solution Chem.* **2009**, *38*, 589.
- (18) Seddon, K.; Stark, A.; Torres, M.-J. *Pure Appl. Chem.* **2000**, *72*, 2275.
- (19) Bhargava, B. L.; Klein, M. L. *Soft Matter* **2009**, *5*, 3475.
- (20) Bhargava, B. L.; Klein, M. L. *Mol. Phys.* **2009**, *107*, 393.
- (21) Zhu, P.; Pratt, L. R.; Papadopoulos, K. D. *J. Chem. Phys.* **2012**, *137*.
- (22) Case, D. A.; T. A. D., Cheatham, T. E., III; Simmerling, C. L.; Wang, J.; Duke, R. E.; Luo, R.; Merz, K. M.; Pearlman, D. A.; Crowley, M.; Walker, R. C.; Zhang, W.; Wang, B.; Hayik, S.; Roitberg, A.; Seabra, G.; Wong, K. F.; Paesani, F.; Wu, X.; Brozell, S.; Tsui, V.; Gohlke, H.; Yang, L.; Tan, C.; Mongan, J.; Hornak, V.; Cui, G.; Beroza, P.; Mathews, D. H.; Schafmeister, C.; Ross, W. S.; Kollman, P. A. *Amber 9*; University of California: San Francisco, CA, 2006.
- (23) Dang, L. X.; Chang, T. M. *J. Phys. Chem. Lett.* **2012**, *3*, 175.
- (24) Dang, L. X.; Chang, T. M. *J. Chem. Phys.* **1997**, *106*, 8149.
- (25) Chang, T. M.; Dang, L. X. *J. Phys. Chem. A* **2009**, *113*, 2127.
- (26) Ciccotti, G.; Ferrario, M.; Hynes, J. T.; Kapral, R. *Chem. Phys.* **1989**, *129*, 241.
- (27) Ciccotti, G.; Ferrario, M.; Hynes, J. T.; Kapral, R. *J. Chem. Phys.* **1990**, *93*, 7137.
- (28) Essmann, U.; Perera, L.; Berkowitz, M. L.; Darden, T.; Lee, H.; Pedersen, L. G. *J. Chem. Phys.* **1995**, *103*, 8577.
- (29) Ryckaert, J. P.; Ciccotti, G.; Berendsen, H. J. C. *J. Comput. Phys.* **1977**, *23*, 327.
- (30) Collins, K. D. *Biophys. J.* **1997**, *72*, 65.
- (31) Collins, K. D. *Methods* **2004**, *34*, 300.
- (32) Collins, K. D. *Biophys. Chem.* **2006**, *119*, 271.
- (33) Fennell, C. J.; Bizjak, A.; Vlachy, V.; Dill, K. A.; Sarupria, S.; Rajamani, S.; Garde, S. *J. Phys. Chem. B* **2009**, *113*, 14837.
- (34) Fennell, C. J.; Bizjak, A.; Vlachy, V.; Dill, K. A. *J. Phys. Chem. B* **2009**, *113*, 6782.
- (35) Hynes, J. T. *Annu. Rev. Phys. Chem.* **1985**, *36*, 573.
- (36) Das, A. K.; Madhusoodanan, M.; Tembe, B. L. *J. Phys. Chem. A* **1997**, *101*, 2862.
- (37) Kramers, H. A. *Physica* **1940**, *7*, 284.
- (38) Grote, R. F.; Hynes, J. T. *J. Chem. Phys.* **1980**, *73*, 2715.
- (39) Nguyen, P. T. M.; Nguyen, V. T.; Annapureddy, H. V. R.; Dang, L. X.; Do, D. D. *Chem. Phys. Lett.* **2012**, *554*, 90.
- (40) Annapureddy, H. V. R.; Dang, L. X. *J. Phys. Chem. B* **2012**, *116*, 7492.
- (41) Rey, R.; Guardia, E. *J. Phys. Chem.* **1992**, *96*, 4712.
- (42) Gertner, B. J.; Wilson, K. R.; Zichi, D. A.; Lee, S.; Hynes, J. T. *Faraday Discuss.* **1988**, *85*, 297.